Electrochimica Acta 220 (2016) 176–183

Contents lists available at ScienceDirect

Electrochimica Acta

journal homepage: www.elsevier.com/locate/electacta

Photo-assisted electrodeposition of a ZnO front contact on a p/n junction

Fabien Tsin[a,d], Dimitrios Hariskos[b], Daniel Lincot[c,d,e], Jean Rousset[a,d,e,*]

[a] EDF R&D, 6 quai Watier, 78401 Chatou Cedex, France
[b] Zentrum für Sonnenenergie-und Wasserstoff-Forschung (ZSW) Baden-Württemberg, Industriestr. 6, D-70565 Stuttgart, Germany
[c] CNRS, 6 quai Watier, 78401 Chatou Cedex, France
[d] IRDEP, Institute of Research and Development for Photovoltaic Energy, UMR 7174, CNRS, EDF, Chimie ParisTech, 78401 Chatou Cedex, France
[e] IPVF, Ile de France Photovoltaic Institute, 8 rue de la Renaissance, 92160 Antony, France

ARTICLE INFO

Article history:
Received 13 July 2016
Received in revised form 13 October 2016
Accepted 15 October 2016
Available online 17 October 2016

Keywords:
ZnO
CIGS
Transparent conductive oxide
Electrodeposition
Solar cell

ABSTRACT

Electrodeposition is an atmospheric and low temperature technique and consequently one of the most interesting way to grow transparent conductive materials at low cost. In this paper the electrodeposition of ZnO films as front contact of a $Cu(In,Ga)(Se,S)_2$ based solar cell is investigated. The electrodeposited ZnO can reach suitable conductivity and transparency for this application. One of the main challenges is to optimize its growth on the p-n junction formed by the $Cu(In,Ga)(Se,S)_2$/CdS stack. Indeed, due to the blocking behavior of this diode in dark conditions, the electrodeposition has to be photo-assisted with an appropriate incident flux. Moreover the growth of a compact film is tricky because of the poor nucleation of ZnO on the CdS surface. As this type of morphology is needed to ensure a sufficient lateral conductivity, we have adapted the electrochemical parameters in order to create a seed layer and improve the density of the nuclei in the first steps of the growth. As a result, with optimized parameters, a contact layer showing a high compactness is reproducibly deposited, leading to a 14.7% efficiency for a $Cu(In,Ga)(Se,S)_2$ based solar cell terminated with an electrodeposited front contact, which is close to the efficiency of the corresponding reference cell with a magnetron sputtered front electrode.

1. Introduction

Zinc oxide has received much attention over the past years due to its numerous applications in such fields as piezoelectric and optoelectronic devices, chemical sensors, photovoltaic applications [1–3]. This work focuses on the application of this transparent conductive oxide (TCO) as the front contact of Cu $(In,Ga)(Se,S)_2$ (CIGS) based solar cell [4,5]. We showed in previous studies that ZnO layers exhibiting high doping levels and intragrain mobilities can be grown by electrodeposition (ED) [6,7]. Two main challenges emerge in transferring the electrodeposition of ZnO from a metallic substrate to a solar cell stack, in our case glass/Molybdenum/CIGS/CdS. The first one is the blocking behavior of the CIGS/CdS diode in dark conditions for cathodic reactions. Therefore this type of substrate has to be illuminated during the growth phase to produce a photocurrent that will be consumed by the electrochemical reaction [8,9]. The second problem is the variation of the compactness of the layer observed as a function of the chemical nature of the substrate. Unfortunately, in the case of a direct deposition on the CdS surface, isolated nuclei are created leading to a three dimensional growth which results in the non-compactness of the deposited layer composed of large sized and disjoint grains. An activation of the CdS surface is then needed to promote the ZnO nucleation. In this paper we present the optimization of the photo-assisted growth by the control of the illumination flux power and the introduction of a seed layer. We apply optimized ED ZnO layers as front contact for CIGS-based solar cells and demonstrate conversion efficiencies close to the efficiency of reference cells with a sputtered ZnO front electrode.

2. Material and methods

The electrodeposition was performed at a low temperature set at 80 °C in a solution containing zinc chloride and potassium chloride with a concentration of 5×10^{-3} M and 0.15 M respectively. The solution was saturated by bubbling oxygen gas used as oxygen precursor [10]. Electrodeposition was performed in a transparent reactor with a three-electrode set-up, using a SP-150

* Corresponding author.
E-mail address: jean.rousset@edf.fr (J. Rousset).

http://dx.doi.org/10.1016/j.electacta.2016.10.102
0013-4686/

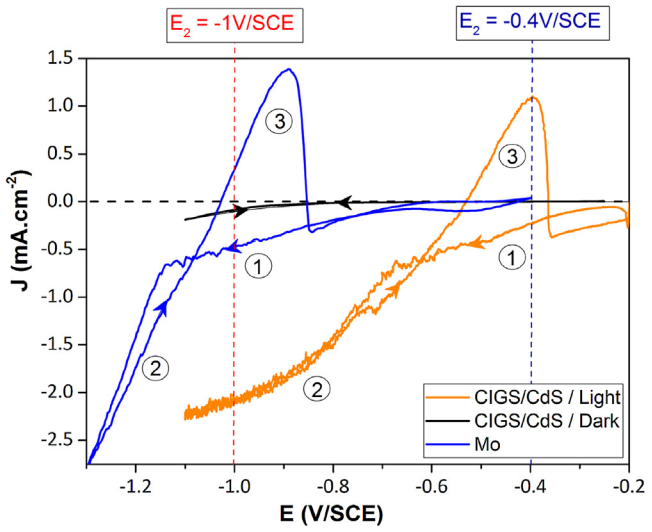

Fig. 1. a) Cyclic voltammetry carried out on a metallic substrate (blue), and on a Cu(In,Ga)(Se,S)$_2$/CdS stack in the dark (black) or under illumination (orange), please refer to the text for the corresponding reactions.

potentiostat from Bio-Logic Science Instruments and the EC-Lab software. The reference electrode was a saturated calomel electrode (SCE +0.248 V vs. normal hydrogen electrode (NHE)). A zinc foil was used as the counter electrode. The CIGS/CdS substrates were grown and provided by ZSW. The two micrometer thick CIGS layer was deposited by coevaporation and covered by a 50 nanometer thick CdS buffer layer deposited by chemical bath deposition.

The ZnO growth is photo-assisted with a light flux produced by a LED (6 mW.cm^{-2}) panel and followed by an annealing at 150 °C for 30 minutes. This annealing step is carried out under low pressure conditions (15 mbar). For the reference cell, a bilayer i-ZnO (50 nm)/ZnO:Al (370 nm) was grown by sputtering on the top of the CIGS/CdS stack. Finally, a zinc metallic grid is electro-deposited according to the procedure described in Ref. [11]

The morphology, composition and thickness of the films were studied by Scanning Electron Microscopy (SEM) using a Zeiss Merlin VP compact microscope coupled with an EDS analyzer. The crystalline structure of the layers was examined by X-ray Diffraction (XRD) with a Panalytical Empyrean X-ray Diffractometer using Cu $K_{\alpha 1}$ radiation (1.5405 Å), in the classical Bragg–Brentano setup.

3. Results and discussion

3.1. Optimization of the incident flux

In order to illustrate the difference between a metallic and a semiconducting substrate, Fig. 1 compares voltamperograms carried out on a glass/molybdenum substrate and on a CIGS/CdS junction.

The current response obtained on the Molybdenum surface is composed by the two electrochemical waves [12] related to the deposition of ZnO (1) from the reduction of O_2 and to the reduction of Zinc ions into metallic Zinc (2). The deposition mechanism of ZnO has been widely studied and is commonly divided into three steps; the reduction of O_2 into hydroxide ions (1a) is followed by the precipitation of the zinc hydroxide (1b) that finally dehydrates as the temperature of the bath is high enough (1c). During the reverse scan, an anodic peak corresponding to the oxidation of the metallic zinc previously deposited (3a) is observed at a potential close to the redox potential of Zn(0)/Zn(II) in this electrolyte. As this electrochemical reaction takes place in a basic environment due to the concomitant reduction of oxygen into hydroxide ions (1a), the zinc ions produced precipitate and form ZnO nuclei at the working electrode according to (3).

$$\frac{1}{2}O_2 + Zn^{2+} + 2e^- \rightarrow ZnO \quad (1)$$

$$\frac{1}{2}O_2 + H_2O + 2e^- \rightarrow 2OH^- \quad (1a)$$

$$Zn^{2+} + 2OH^- \rightarrow Zn(OH)_2 \quad (1b)$$

$$Zn(OH)_2 \rightarrow ZnO + H_2O \quad (1c)$$

$$Zn^{2+} + 2e^- \rightarrow Zn \quad (2)$$

$$Zn \rightarrow Zn^{2+} + 2e^- \quad (3a)$$

$$Zn + 2OH^- \rightarrow ZnO + 2e^- + H_2O \quad (3)$$

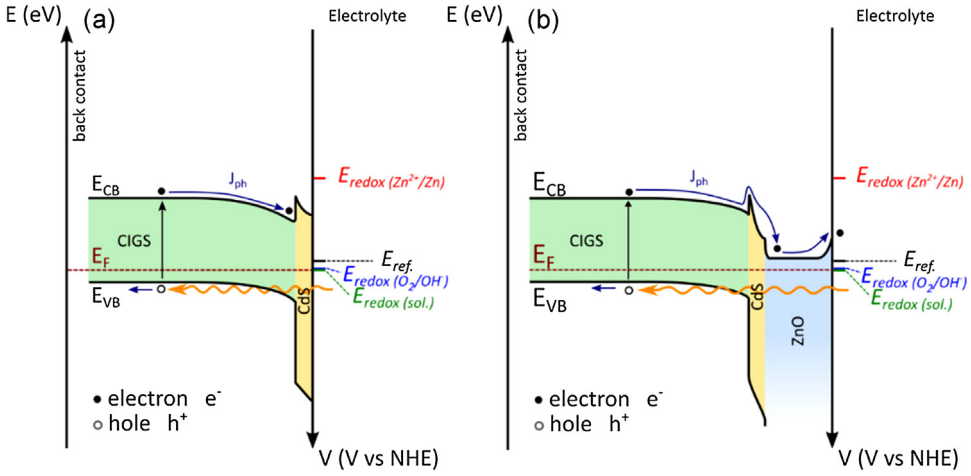

Fig. 2. (a) Band diagram of a CIGS/CdS p/n junction stack in contact with the electrolytic bath. (b) Band diagram of a Mo/CIGS/CdS/ZnO stack in contact with the electrolyte at open circuit potential.

In a case of a semiconducting substrate, when the solid and the liquid phases are put into contact, the alignment of the Fermi level of semiconductor with the redox potential of the solution occurs leading to the creation of a voltage drop.

The band diagram of the CIGS/CdS stack in contact with the electrolyte has been calculated with the software SCAPS and is presented in Fig. 2 assuming that the redox level of the electrolyte is that of the oxygen/hydroxide electrochemical couple. In Fig. 2b we have considered the presence of doped zinc oxide on the top of CdS. In that case a very thin ZnO/electrolyte junction is formed at the interface. On the Mo/CIGS/CdS substrate, the electrochemical cathodic current measured in dark conditions is much lower than that observed on the Molybdenum surface in the same potential range (black curve in Fig. 1). This is due to the p-type semiconducting character of CIGS which forms a blocking junction for reduction reaction. When the interface is illuminated, the supply of photo-generated electrons at the liquid/solid interface leads to the measurement of the electrochemical features described above (orange curve in Fig. 1). The main difference with the metal substrate is the shift, of about 0.5 V, of the electrochemical phenomena towards less negative potentials. Therefore the potentials applied during the growth have to be adapted as the function of the substrate nature. The photo-generated electrons are injected at the energy level of the

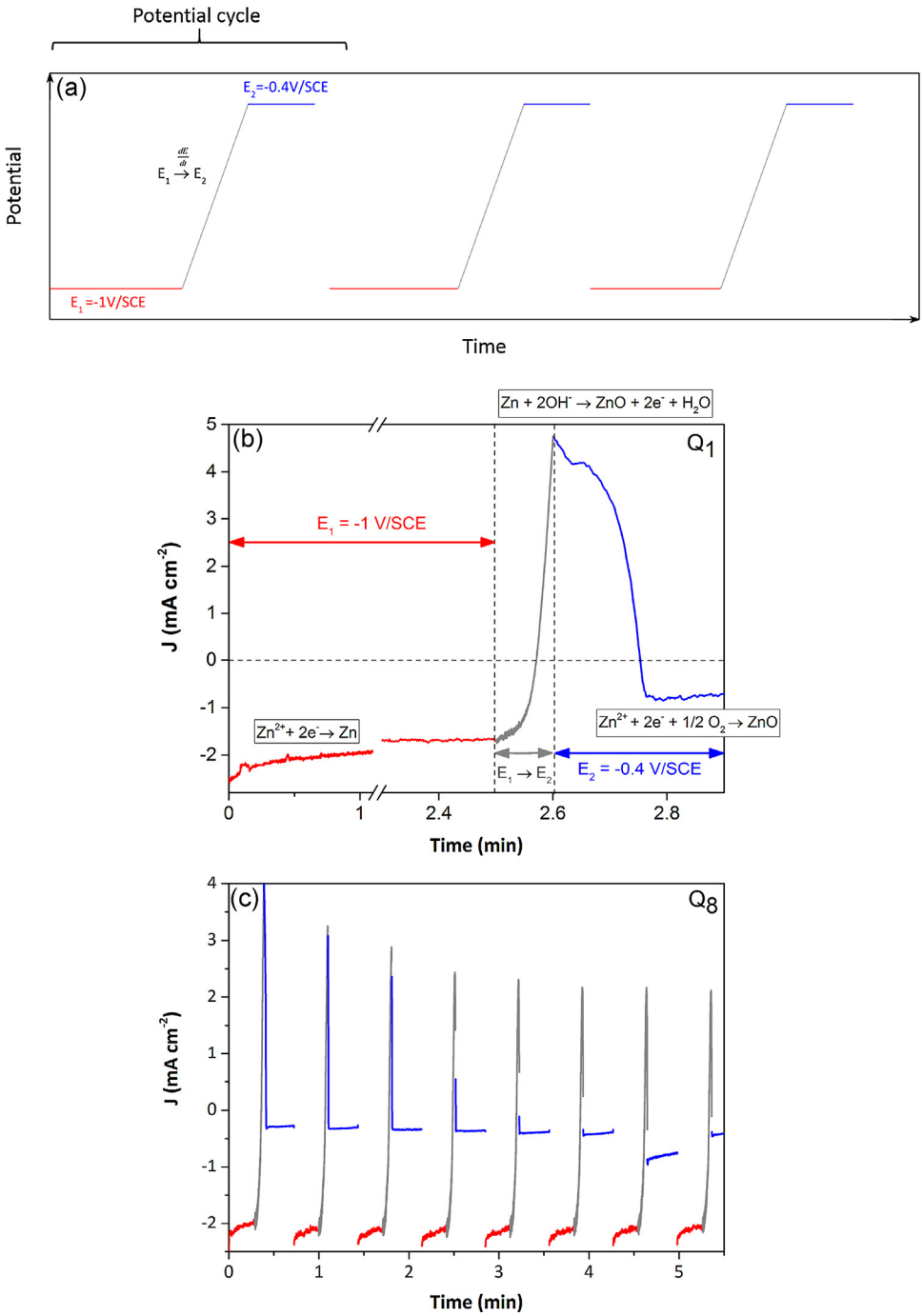

Fig. 3. (a) Description of the potential cycle applied during the seed layer deposition Current responses measured with one cycle (method Q1) (b) and eight cycles (c) (method Q8).

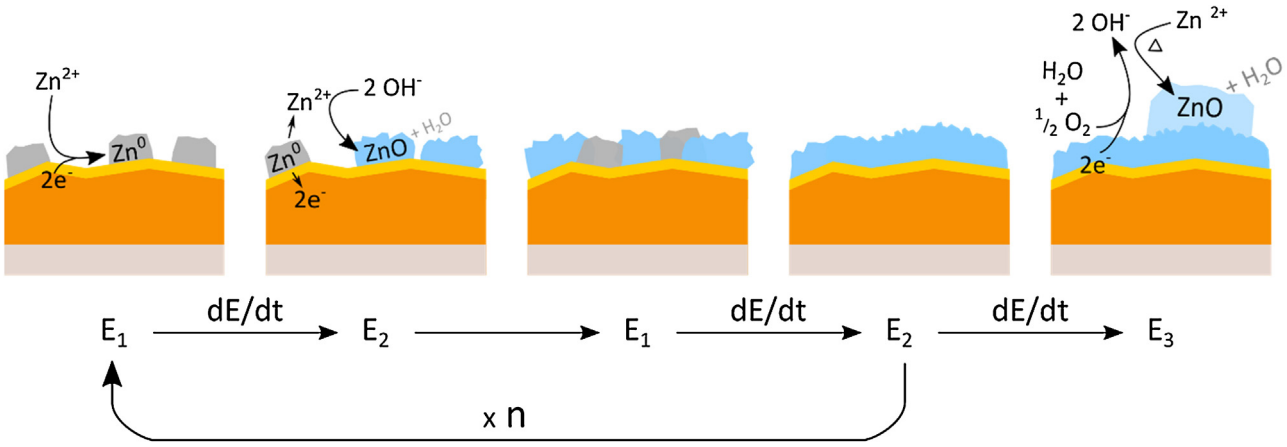

Fig. 4. Schematic representation of the seed layer formation.

conduction band of the semiconductor, that means at a very cathodic potential, at the interface with the electrolyte. This energy transfer from the incident light to the electrochemical system leads to the observed potential shift. According to the band diagram the reduction potential of O_2 into hydroxide ions is less negative than the conduction band position. Thus the photo-generated electrons are consumed at the CdS surface and are able to reduce the oxygen dissolved in the electrolyte. The deposition of the ZnO is even possible under illumination without external potential applied at the working electrode. On the contrary, from a thermodynamic point of view, the reduction of the zinc ions into metallic zinc should not be possible since the redox potential of the zinc is lower than that of the conduction band at the interface. Nevertheless this reaction is experimentally observed. To explain this phenomenon one should consider a variation of the band position at the liquid/solid interface [13]. If the carriers produced under illumination are

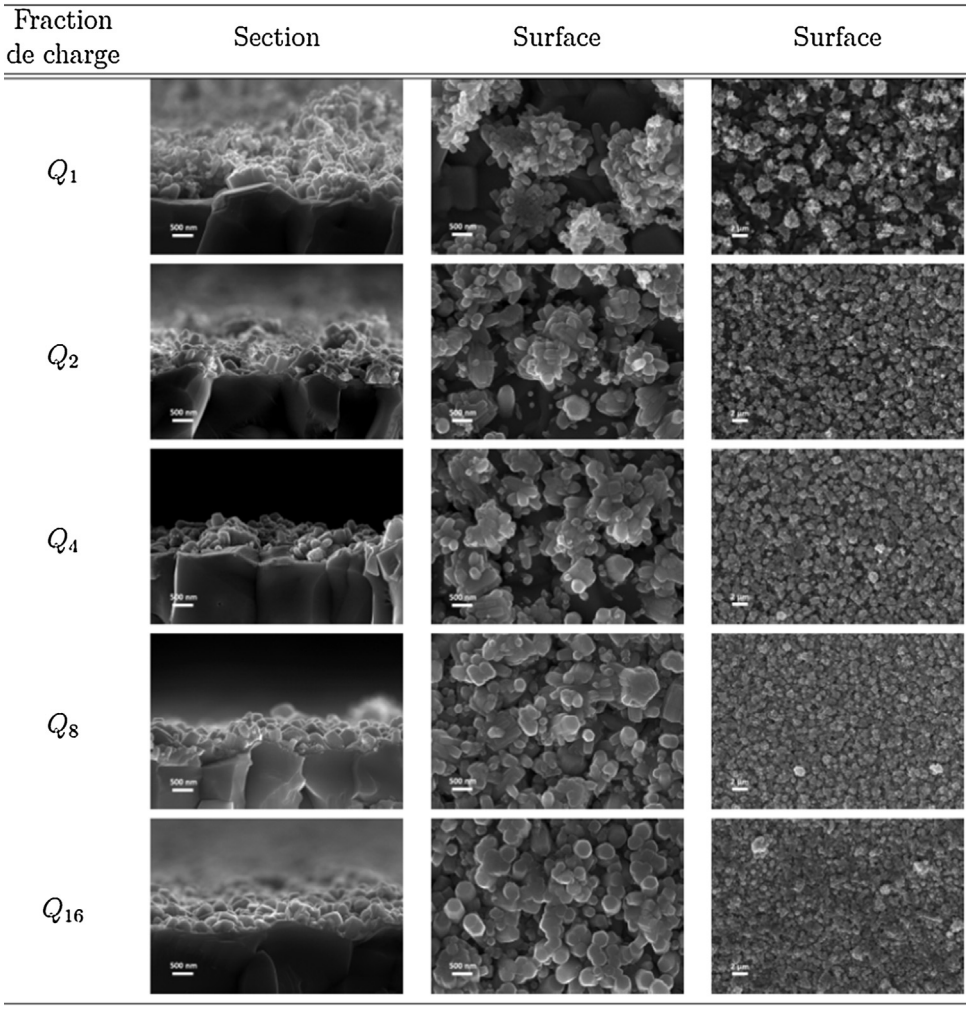

Fig. 5. SEM Images of the seed layers deposited under different experimental conditions (from Q1 to Q16).

not fully consumed by the electrochemical reaction, they are expected to accumulate at the semiconductor surface. This negative charge is compensated at the liquid interface by the positive ions present in solution. Due to the presence of the Helmholtz layer which behaves as an insulator an interfacial capacity appears that is expected to create an additional negative potential. This potential leads to a conduction band shift at the semiconductor surface towards more negative values enabling the reduction of the zinc ions into metallic zinc. The power of the incident flux is another parameter to optimize. In the case of a metallic substrate the reduction current and consequently the growth rate of the ZnO layer is mainly limited by the oxygen diffusion from the solution bulk to the working electrode and depends on the convection regime in the electrolyte. In the case of a photo-assisted deposition two situations are possible for a set hydrodynamic regime. If the incident flux power is high enough to produce a photocurrent higher than the diffusion limited current, the reduction rate is the same as that obtained on a metallic substrate. Otherwise the growth rate is function of the illumination power. In the presented case we set the incident power at a value that allows to roughly match the photocurrent and the electrochemical one. On the one hand, the current density value expected for this electrochemical system is in the range of the milliamp by centimeter square. One the other hand, the photocurrent produced in the CIGS layer is proportional to the incident light power and reaches values close to 30 mA.cm^{-2} under AM 1.5 illumination (namely 100 mW.cm^{-2}). The power of the incident light was set to 6 mW.cm^{-2} during the photo-assisted electrodeposition. This value is high enough to obtain a photocurrent (1.8 mA.cm^{-2}) slightly superior to that needed for the O_2 reduction.

3.2. Optimization of electrochemical parameters

3.2.1. Optimization of the seed layer

In order to increase the compactness and consequently the lateral conductivity of the ZnO film, the growth of a seed layer achieved by simply playing on the applied potential is investigated. The growth process was divided into two steps. The first one (seed layer) consists of the growth of a dense seed layer and is followed by a deposition at a controlled potential (deposition step). This approach is inspired by a previous work published by Canava et al. [14] where the application of a very reducing potential has been demonstrated to enhance the nucleation of ZnO on a SnO_2 surface. Thus, in order to boost the nucleation on the CdS surface, potential cycles that alternate the application of reducing and oxidizing potential with respect to the zinc redox couple are applied during the seed layer growth. The shape of the potential cycles and the related current response of the electrochemical system are presented in Fig. 3.

First a potential $E_1 = -1$ V/SCE lower than that of the zinc reduction is applied during a given consumed charge (Q_n) leading to the creation of metallic zinc nuclei on the CdS surface. Then the potential is progressively shifted to a higher (less reducing) value ($E_2 = -0.4$ V/SCE) with a scan rate of 100 mV.s^{-1}. Finally this latter potential is applied for 20 s leading to the reoxidation of the metallic zinc and to the formation of ZnO nuclei according to the

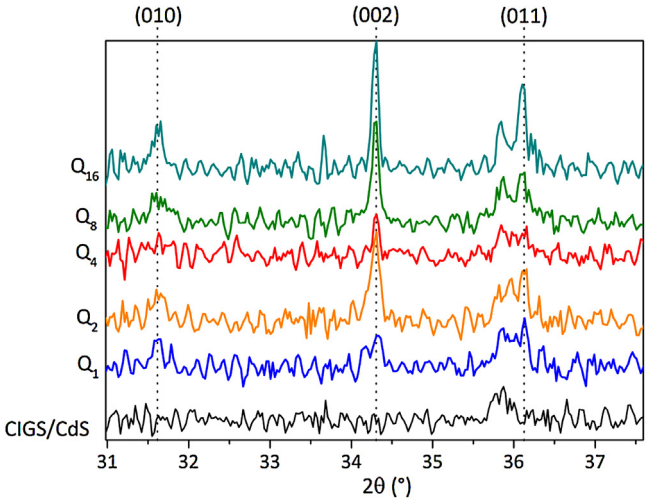

Fig. 6. XRD diagrams of the seed layers deposited under different experimental conditions (from Q1 to Q16).

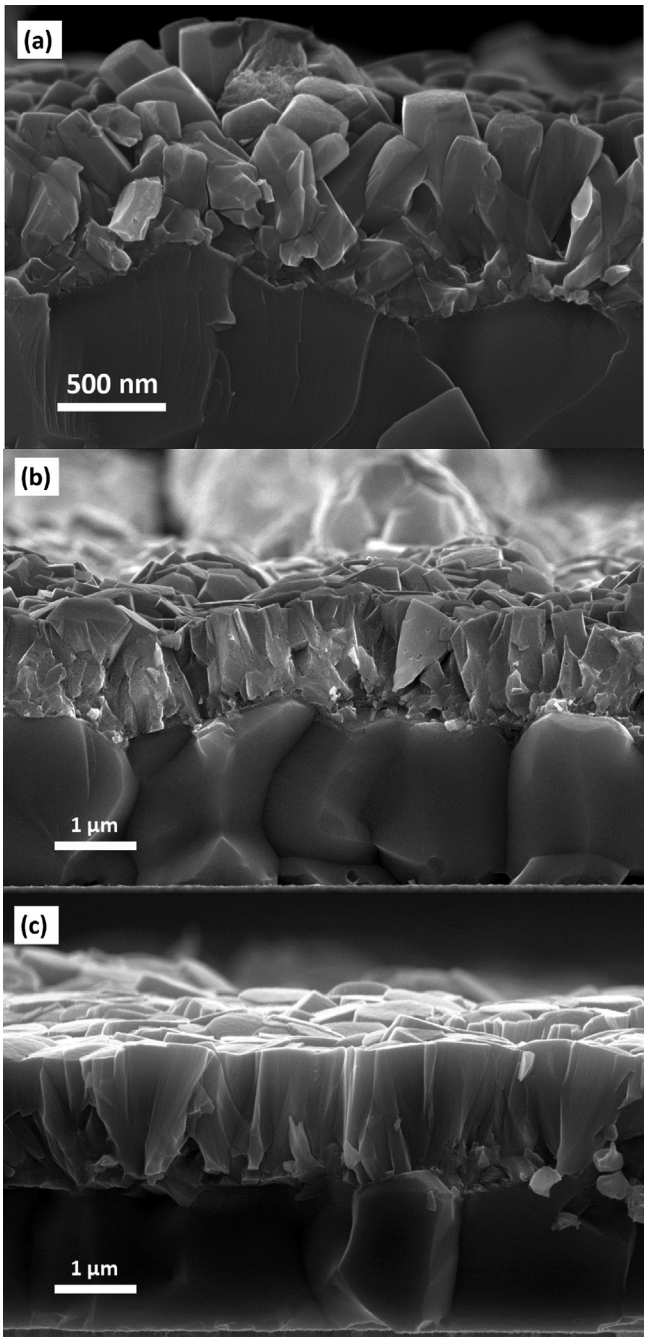

Fig. 7. SEM images of the cross section of ZnO layers obtained without seed layer (a), with a seed layer deposited in the conditions Q6 (b) and with a seed layer deposited in the conditions Q6 and a variable potential applied during the deposition step (c).

global reaction (3). This mechanism is illustrated with the sketch presented in Fig. 4.

The current response (Fig. 3) measured during one cycle is in accordance with this scenario. Indeed a cathodic current is measured during the first step due to the reduction of zinc ions into metallic zinc. During the second step an anodic current appears and progressively decreases in absolute value with time until all the metallic zinc is oxidized. Finally the current stabilizes at a negative value corresponding to the reduction of O_2 into hydroxide ions. The influence of the number of cycles has been studied. The principle is to keep the total charge consumed constant as the potential is set at E2 (Q_{tot}) and to increase the number of cycles. If a seed layer is deposited in n cycles the charge consumed per cycle at E_2 is set at $Q_n = Q_{tot}/n$. Q_{tot} has been set at 80 mAh.cm^{-2} (288 mC.cm^{-2}) corresponding to a total theoretical metallic Zinc thickness of 137 nm. Fig. 3b and 3c show the current responses obtained for one and eight cycles (Q_8 = 10 mAh.cm^{-2}) respectively. The morphology of the seed layers obtained under the different tested experimental conditions are shown in Fig. 5. As a unique cycle is carried out, the seed layer is composed of isolated and randomly oriented ZnO grains. The increase of the number of cycles from Q1 to Q8 leads to a densification of the seed layer and makes it more covering. The further decrease of the charge per cycle has no additional effect on the seed layer growth.

Moreover the enhancement of the crystalline quality of the film with the shortening of the cycle is clearly visible in the XRD diagram presented in Fig. 6. The [002] XRD peak of the Wurtzite structure clearly appears with the decrease of the charge consumed per cycle. This observation is consistent with the evolution of the seed layer morphology. Indeed the grains become more ordered and start to adopt the classical hexagonal shape of the electrodeposited ZnO layer with its typical orientation along the c-axis of the wurtzite structure.

The presence of the seed layer clearly impacts the final ZnO morphology when the growth is terminated by a potentiostatic deposition step. The compactness of the film is greatly enhanced as shown in Fig. 7.

3.2.2. Improvement of the deposition step

For the deposition step, two different methods have been tested and compared. The method 1 consists in the application of a constant potential set at $E = -0.7$ *V/SCE*. This potential is situated at the lower limit of the oxygen reduction plateau and is just slightly superior to the potential of the Zinc ions reduction. The current response as the function of time obtained in this case is shown in Fig. 8. The current density varies from -1 mA.cm^{-2} to -0.25 mA.cm^{-2}. This evolution is not fully understood yet but cannot originate from an additional resistance produced by the growth of the ZnO layer, due to the very high conductivity of this layer [6]. In order to compensate this current drop the applied potential can be gradually shifted towards more reducing potential during the deposition (Method 2). In the case presented in Fig. 8, the rate scan, the start and final potentials have been set to 0.1 mV.s^{1}, -0.6 V/SCE and -0.8 V/SCE respectively. These values have been empirically

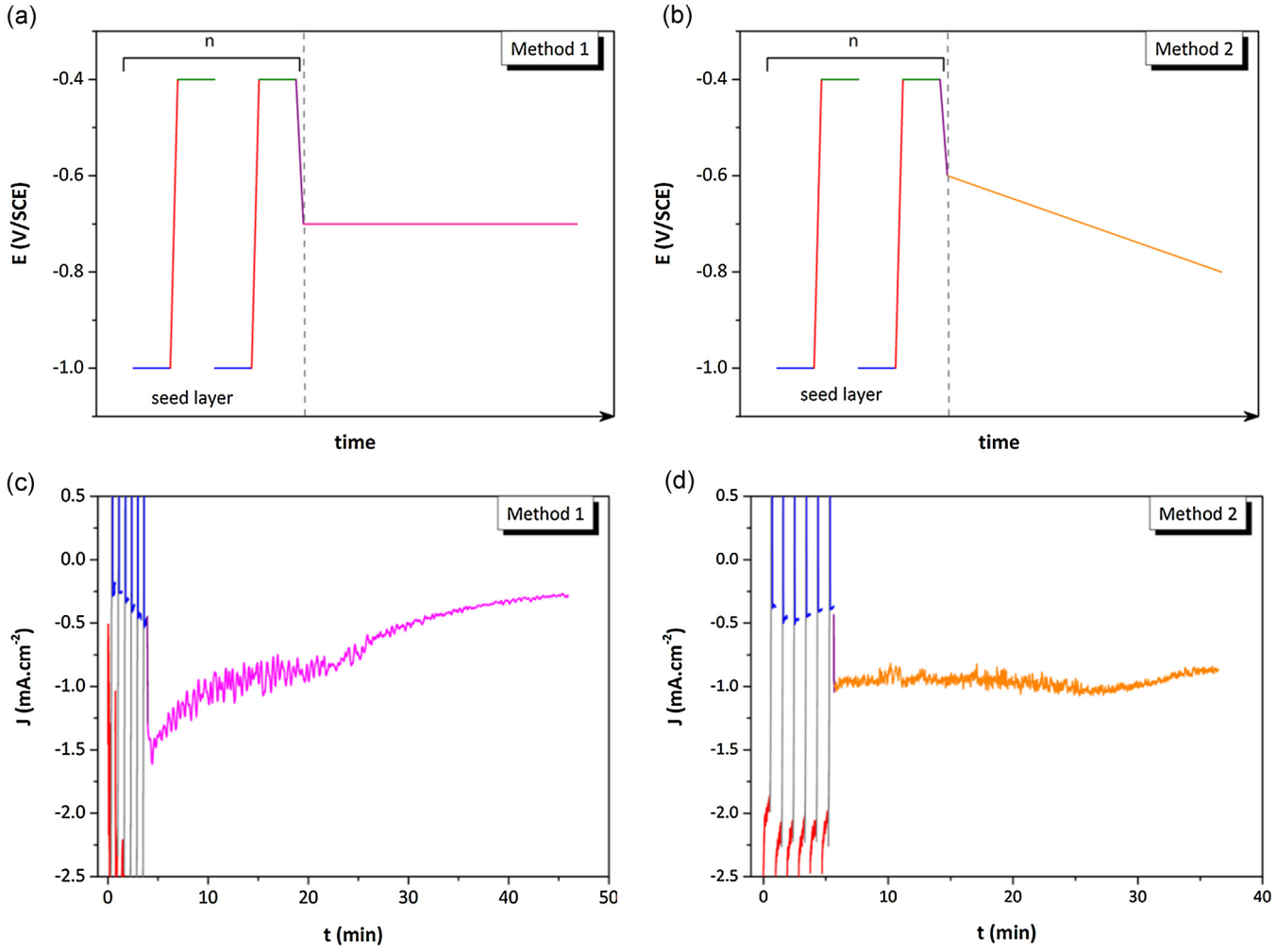

Fig. 8. Description of the growth process including a potentiostatic (a) or potentiodynamic deposition step (b) and their related current response (c) and (d).

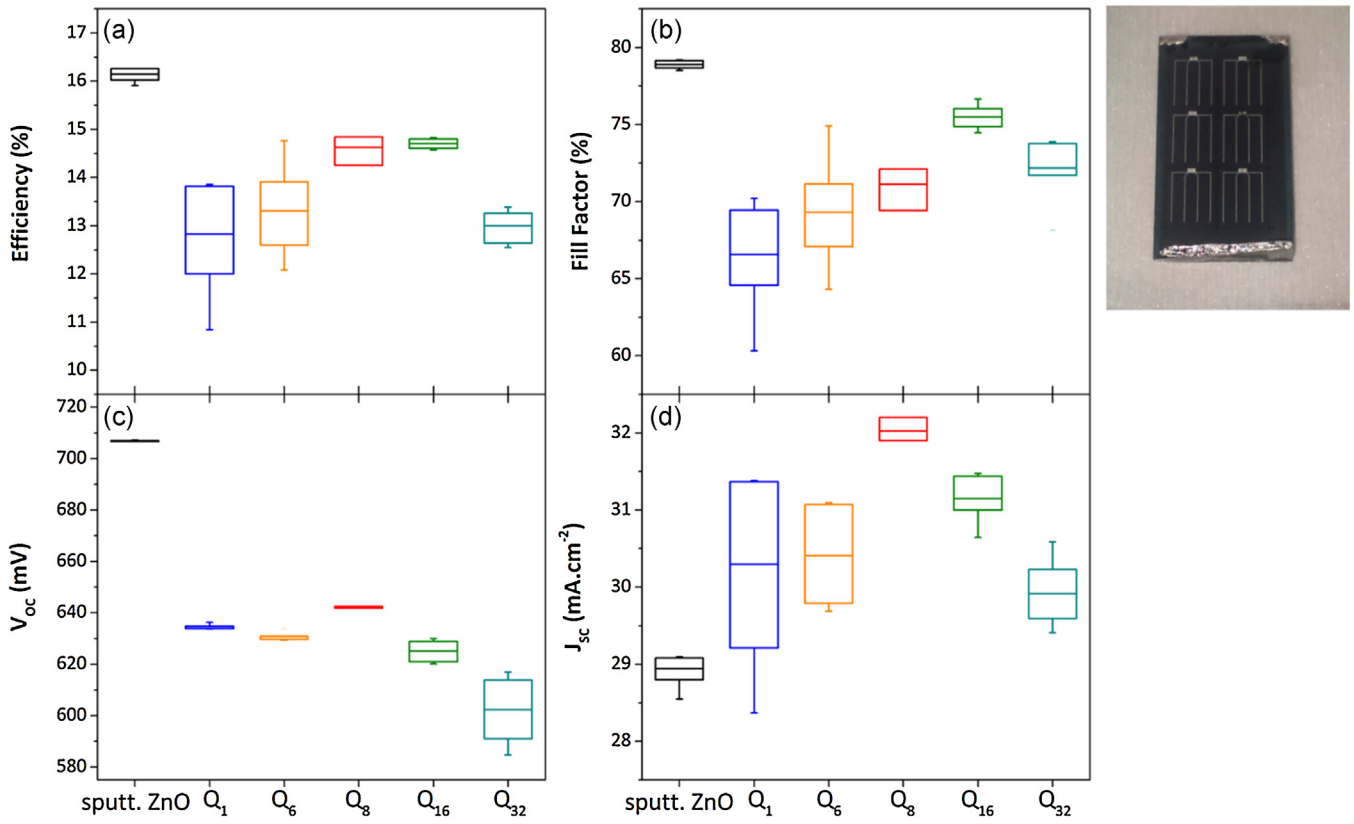

Fig. 9. Electrical parameters of the solar cells obtained with different seed layers. The performances obtained with the reference sputtered ZnO layer appear in black. The photography shows a sample divided into six 0.5 cm^2 CIGS solar cells terminated with an electrodeposited ZnO and an electrodeposited Zinc metallic contact.

chosen according to the efficiency measured on the complete cell as selection criterion. The potential shape presented in Fig. 8b leads to a current density that remains constant (close to −1 mA.cm^{-2}) during the whole deposition step. This method presents two main advantages. Firstly, the constant current allows to decrease the total duration of the growth; 30 minutes for a 1.30 μm to be compared to 40 minutes in the case of a constant applied potential. Secondly the layer deposited with the method 2 (Fig. 4c) shows a higher compactness and a more ordered morphology than those obtained in potentiostatic conditions (Fig. 4b).

3.3. Performance of the electrodeposited layer as front contact of a CIGS based solar cell

CIGS based solar cells with a 1.3 micron thick electrodeposited ZnO front contact, obtained with seed layers grown under different conditions, have been tested. The total charge consumed during the seed layer deposition is kept constant and is divided in 6, 8, 16 or 32 cycles. After this first step the deposition is carried out applying a variable potential as described above.

The light conversion efficiency has been measured on samples divided into six 0.5 cm^2 cells and terminated by a metallic grid. The electrical parameters are shown in Fig. 9. As the same material stack is used for all the investigated conditions, the variations are expected to originate only from the properties of the front contact. The final efficiency of the solar cell is greatly impacted by the deposition conditions of the ZnO layer and varies from 12.8% to 14.7% depending on the charge consumed per cycle. These efficiencies remain lower than those obtained with the classical sputtered bi-layer (16% with a 50 nm thick intrinsic ZnO covered by a 350 nm thick Al-doped ZnO) but demonstrate that the electrodeposited material shows interesting optoelectronic properties for this application. The decrease of the cycle duration mainly affects the fill factor of the cell which ranges from 66.6% to 75.5%. This improvement is clearly related to the variation of the ZnO morphology with the deposition conditions, as shown above. Indeed, for the shorter cycles the high density of nuclei formed leads to the enhancement of the compactness and crystallinity of the material. This evolution is expected to increase the lateral of the carrier in the front contact decreasing its lateral resistivity. As a result the fill factor which is very sensitive to the sheet resistivity of this layer is enhanced. Moreover, the principal loss measured with

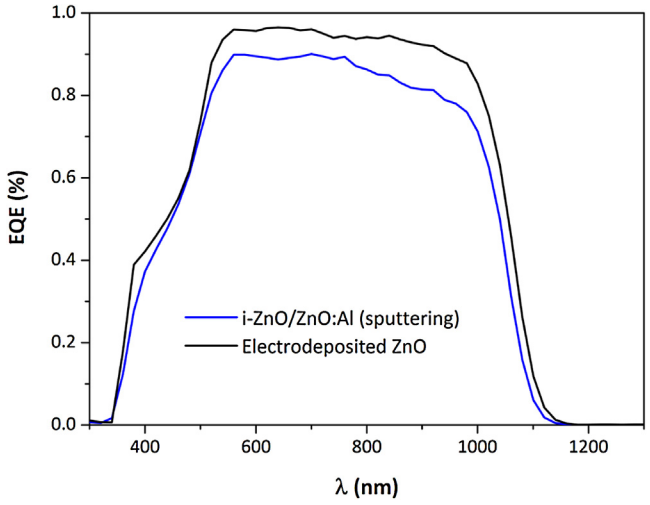

Fig. 10. Quantum efficiency of a CIGS solar cell terminated with an electrodeposited front contact (condition Q8) and with a sputtered ZnO bilayer.

an electrodeposited front contact compared to the cell terminated with a sputtered one is mainly seen in the open circuit voltage with a difference ranging from 65 mV to 105 mV depending on the deposition condition. This difference can originate from the possible photoreduction of a part of the CdS buffer layer during the first moments of the deposition or from the absence of a ZnO intrinsic layer in the cell stack. On the contrary the cell terminated by an electrodeposited shows a significantly higher short circuit.

The external quantum efficiency obtained with an electrodeposited contact reaches values up to 96% and is globally higher than that measured with a sputtered bilayer (Fig. 10). This improvement can be firstly related to the higher transparency of the electrodeposited material in particular in the near infrared domain. This effect is due to a lower doping level leading to a lower free carrier absorption. Secondly the electrodeposited layer shows a higher roughness that may decrease the light reflection at the cell surface.

4. Conclusion

In this paper, we have shown that a fine control of the parameters during ZnO photo-assisted electrodeposition allows to obtain layer suitable for solar cell front contact applications. The power of the incident light has been optimized in order to produce a photocurrent that matches well with that consumed by the electrochemical reaction. We also demonstrated that the compactness of the layer can be tuned adapting the applied potential: first a seed layer is deposited and is followed by a ZnO deposition with a variable applied potential. With a fully optimized layer an efficiency comparable to that obtained with a sputtered contact layer was measured.

Acknowledgments

The authors would like to thank Dr. Julien Vidal and Misheal Stanley for manuscript correction. The authors are grateful to the support from the SOLAR-ERA.NET European program in framework of NovaZolar project.

References

[1] Ü. Özgür, Y.I. Alivov, C. Liu, A. Teke, M.A. Reshchikov, S. Doğan, V. Avrutin, S.-J. Cho, H. Morkoç, A comprehensive review of ZnO materials and devices, J. Appl. Phys. 98 (2005) 04131, doi:http://dx.doi.org/10.1063/1.1992666.
[2] A. Mills, S. Le Hunte, An overview of semiconductor photocatalysis, J. Photochem. Photobiol. A Chem. 108 (1997) 1–35.
[3] C. Klingshirn, ZnO: Material, Physics and Applications, ChemPhysChem. 8 (2007) 782–803, doi:http://dx.doi.org/10.1002/cphc.200700002.
[4] H. Hagendorfer, K. Lienau, S. Nishiwaki, C.M. Fella, L. Kranz, A.R. Uhl, D. Jaeger, L. Luo, C. Gretener, S. Buecheler, Y.E. Romanyuk, A.N. Tiwari, Highly Transparent and Conductive ZnO: Al Thin Films from a Low Temperature Aqueous Solution Approach, Adv. Mater. 26 (2014) 632–636, doi:http://dx.doi.org/10.1002/adma.201303186.
[5] F. Tsin, A. Venerosy, J. Vidal, S. Collin, J. Clatot, L. Lombez, M. Paire, S. Borensztajn, C. Broussillou, P.P. Grand, S. Jaime, D. Lincot, J. Rousset, Electrodeposition of ZnO window layer for an all-atmospheric fabrication process of chalcogenide solar cell, Sci. Rep. 5 (2015) 8961, doi:http://dx.doi.org/10.1038/srep08961.
[6] J. Rousset, E. Saucedo, D. Lincot, Extrinsic doping of electrodeposited zinc oxide films by chlorine for transparent conductive oxide applications, Chem. Mater. 21 (2009) 534–540.
[7] J. Rousset, E. Saucedo, K. Herz, D. Lincot, High efficiency CIGS-based solar cells with electrodeposited ZnO: Cl as transparent conducting oxide front contact, Prog. Photovoltaics Res. Appl. 19 (2011) 537–546, doi:http://dx.doi.org/10.1002/pip.
[8] K. Uno, Y. Tauchi, I. Tanaka, ZnO Thick Film Growth on n-GaN by Photoassisted Electrodeposition, Jpn. J. Appl. Phys. (2013) 08JE16.
[9] M. Zamzuri, J. Sasano, F. Binti, M. Izaki, Substrate type b 111 N –Cu 2 O/b 0001 N –ZnO photovoltaic device prepared by photo-assisted electrodeposition, Thin Solid Films 595 (2015) 136–141, doi:http://dx.doi.org/10.1016/j.tsf.2015.10.054.
[10] S. Peulon, D. Lincot, Cathodic electrodeposition from aqueous solution of dense or open-structured zinc oxide films, Adv. Mater. 8 (1996) 166–170, doi:http://dx.doi.org/10.1002/adma.19960080216.
[11] F. Tsin, J. Rousset, A. Le Bris, D. Lincot, Electrodeposited zinc grid as low-cost solar cell front contact, Prog. Photovoltaics Res. Appl. (2016), doi:http://dx.doi.org/10.1002/pip.2778.
[12] S. Peulon, D. Lincot, Mechanistic study of cathodic electrodeposition of zinc oxide and zinc hydroxychloride films from oxygenated aqueous zinc chloride solutions, J. Electrochem. Soc. 145 (1998) 864–874.
[13] D. Lincot, J. Vedel, Recombinaison and charge transfer at the illuminated n-CdTE/electrolyte interface: simplfied kinetic model, J. Electroanal. Chem 220 (1987) 179–200.
[14] B. Canava, D. Lincot, Nucleation effects on structural and optical properties of electrodeposited zinc oxide on tin oxide, J. Appl. Electrochem. 30 (2000) 711–716, doi:http://dx.doi.org/10.1023/A:1003857026200.